K-shell Photoabsorption of Oxygen Ions

J. García, C. Mendoza, M. A. Bautista,

Centro de Física, IVIC, Caracas 1020A, Venezuela

jgarcia@ivic.ve; claudio@ivic.ve; bautista@ivic.ve

T. W. Gorczyca,

Department of Physcics, Western Michigan University, Kalamazoo, MI 49008

thomas.gorczyca@wmich.edu

T. R. Kallman, and P. Palmeri[1]

NASA Goddard Space Flight Center, Greenbelt, MD 20771

timothy.r.kallman@nasa.gov; palmeri@milkyway.gsfc.nasa.gov

ABSTRACT

Subject headings: atomic processes — atomic data — line formation — X-rays: general

1. Introduction

The high spectral resolutions of the *Chandra* and *XMM-Newton* X-ray observatories have unveiled the useful diagnostic possibilities of oxygen K absorption. To mention a few, strong O VII and O VIII edges are almost ubiquitous in the spectra of Seyfert 1 galaxies which have been used by Lee et al. (2001) to predict of a warm dust absorber along the line of sight; although this conclusion has been criticized in the light of a data reanalysis (Sako et al. 2003), Steenbrugge et al. (2003) have detected inner-shell transitions of O III–O VI in the spectrum of NGC 5548 that point to a warm absorber that spans three orders of magnitude in ionization parameter. Moreover, Behar et al. (2003) have stressed that, in the case of both

[1]Research Associate, Department of Astronomy, University of Maryland, College Park, MD 20742.

Seyfert 1 and Seyfert 2 galaxies, a broad range of oxygen charge states are usually observed along the line of sight that must be fitted simultaneously, and may imply strong density gradients of 2–4 orders of magnitude over short distances.

Schulz et al. (2002) have reported that the spectrum of the archetypical black hole candidate Cyg X-1 shows a prominent oxygen K edge that when modelled suggests a deficient O abundance approximately consistent with an abundance distribution in the interstellar medium (ISM). Observations of the O I edge and the equivalent widths of O II–O VIII in the spectrum of the black-hole binary LMC X-3 by Page et al. (2003) lead to upper limits of the neutral and ionized column densities that rule out a line-driven stellar wind, and thus suggest a black body with a multi-temperature disk. A gravitationally redshifted O VIII Lyα observed in absorption in the spectrum of the bursting neutron star EXO 0748-676 shows, unlike Fe ions, multiple components consistent with a Zeeman splitting in a magnetic field of around $1–2\times10^9$ G (Loeb 2003). Sako (2003) has shown that, in optically thick conditions, an O VIII–N VII Bowen fluorescence mechanism, caused by the wavelength coincidence of the respective Lyα (2p–1s) and Lyζ (7p–1s) doublets, can suppress O emission while enhancing C and N thus leading to abundance misinterpretations.

The 1s–2p resonant absorption lines from O ions with electron occupancies $N \leq 3$ are being used with comparable efficiency in the detection of the warm-hot intergalactic medium which, according to simulations of structure formation in the Universe, contains most of the baryons of the present epoch (Cagnoni et al. 2004). A spectral comparison of low and high extinction sources can lead to the separation of the ISM and instrumental components of the K edge (de Vries et al. 2003), the former closely resembling the edge structure of neutral oxygen computed by McLaughlin & Kirby (1998) with the R-matrix method (Berrington et al. 1987; Seaton 1987). High-resolution spectroscopy of the interstellar O K edge in X-ray binaries have been carried out by Juett et al. (2004), disclaiming previously proposed oxygen features from dust and molecular components and providing the first estimates of the O ionization fractions.

Accurate laboratory wavelength measurements for K-shell resonance lines in O VII have been reported by Engström & Litzén (1995) using laser pulses focused on compressed powder targets and by Beiersdorfer et al. (2003) with an electron beam ion trap; the latter method has been extended recently to O VI and O V (Schmidt et al. 2004). K-shell photoabsorption of O I has been measured by Menzel et al. (1996) and (Stolte et al. 1997), and of O II by Kawatsura et al. (2002) where the role of theoretical data—namely level energies, wavelengths, gf-values, and natural widths—in experimental interpretation has been emphasized. Laboratory energies for K-vacancy states in O I and O II have been obtained by Auger electron spectrometry (Caldwell & Krause 1993; Krause 1994; Caldwell et al. 1994),

but worrisome discrepancies with the photoabsorption measurements have not as yet been settled.

Such experimental activity has certainly encouraged theoretical verifications which have employed a variety of atomic structure and close-coupling approaches. Radiative and Auger data related to the satellite lines of H-, He-, and Li-like oxygen have been computed in an approach based on the $1/Z$ hydrogenic expansion (Vainshtein & Safranova 1971, 1978) and with the multiconfiguration Dirac–Fock method (Chen 1985, 1986). A theoretical study of the K-shell Auger spectrum of O I has been carried out with the multiconfiguration Hartree–Fock method (Saha 1994) finding good agreement with the measurements by Caldwell & Krause (1993). Energy positions and total and partial Auger decay rates for the $[1s]2p^4\ ^4P$ and ^2P terms of O II have been determined by Petrini & Araújo (1994) with the structure code SUPERSTRUCTURE (Eissner et al. 1974) and PHOTUC (Saraph 1987), the latter being based on an implementation of the close-coupling approximation of scattering theory. The K-shell photoionization cross section of the ground state of neutral oxygen has been computed with the R-matrix method by McLaughlin & Kirby (1998), giving a detailed comparison with the experimental energy positions for the $[1s]2p^4(^4P)np\ ^3P^o$ and $[1s]2p^4(^2P)np\ ^3P^o$ Rydberg series. More recently, the R-matrix method has also been used to compute the high-energy photoionization cross section of: the ground states of O VI in an 11-state approximation (Charro et al. 2000); O I taking into account core relaxation effects and the Auger smearing of the K edge (Gorczyca & McLaughlin 2000b); and in its relativistic Breit–Pauli mode, O I–O VI whereby wavelengths and f-values are obtained for the $n = 2$ Kα resonance complexes with $f > 0.1$ (Pradhan et al. 2003).

We are presently interested in a realistic modelling of the oxygen K edge and in formally establishing its diagnostic potential. For this purpose we have computed as accurately as possible the required atomic data, some of which are not available for the whole O sequence, and used the XSTAR photoionization code (Kallman & Bautista 2001). Previous models have been fitted with two absorption edges and five Gaussian absorption lines (Juett et al. 2004). The present data sets have been computed in a systematic approach previously used for the iron isonuclear sequence (Bautista et al. 2003; Palmeri et al. 2003a,b; Bautista et al. 2004; Mendoza et al. 2004) which has allowed the determination of the efficiency of Fe K line emission and absorption in photoionized models (Kallman et al. 2004).

2. Numerical methods

The numerical approach has been fully described in Bautista et al. (2003). The atomic data, namely level energies, wavelengths, gf-values, radiative widths, total and partial

Auger widths, and total and partial photoionization cross sections are computed with a portfolio of publicly available atomic physics codes: AUTOSTRUTURE, HFR, and BPRM. Although relativistic corrections are expected to be negligible for the lowly ionized species of the O sequence, they can be more conspicuous for members with greater effective charge $z = Z - N + 1$, Z being the atomic number and N the electron occupancy. For consistency, wavefunctions are calculated, unless otherwise stated, with the relativistic Breit–Pauli Hamiltonian

$$H_{\rm bp} = H_{\rm nr} + H_{\rm 1b} + H_{\rm 2b} \tag{1}$$

where $H_{\rm nr}$ is the usual non-relativistic Hamiltonian. The one-body relativistic operators

$$H_{\rm 1b} = \sum_{n=1}^{N} f_n({\rm mass}) + f_n({\rm d}) + f_n({\rm so}) \tag{2}$$

represent the spin–orbit interaction, $f_n({\rm so})$, the non-fine-structure mass variation, $f_n({\rm mass})$, and the one-body Darwin, $f_n({\rm d})$, correction. The two-body Breit operators are given by

$$H_{\rm 2b} = \sum_{n<m} g_{nm}({\rm so}) + g_{nm}({\rm ss}) + g_{nm}({\rm css}) + g_{nm}({\rm d}) + g_{nm}({\rm oo}) \tag{3}$$

where the fine-structure terms are $g_{nm}(so)$ (spin–other-orbit and mutual spin-orbit), $g_{nm}(ss)$ (spin–spin), and the non-fine-structure counterparts $g_{nm}(css)$ (spin–spin contact), $g_{nm}(d)$ (two-body Darwin), and $g_{nm}(oo)$ (orbit–orbit).

Brief outlines of the programs are given as follows specially in connection with the approximations used.

2.1. AUTOSTRUCTURE

AUTOSTRUCTURE (Badnell 1986, 1997) computes fine-structure level energies, radiative, and Auger rates in a Breit–Pauli framework including to order $\alpha^2 Z^4$ the one- and two-body operators in Eq. (3), α being the fine-structure constant. This code may be regarded as an extension of the SUPERSTRUCTURE atomic structure package (Eissner et al. 1974) wherein configuration interaction (CI) wavefunctions of the type

$$\Psi(LS) = \sum_i c_i \phi_i \tag{4}$$

are constructed from single-electron orbitals generated in a statistical Thomas–Fermi–Dirac potential and optimized variationally. Continuum wavefunctions are constructed within the distorted-wave approximation. Core relaxation effects (CRE) are investigated by comparing

an ion representation where all electron configurations have a common basis of orthogonal orbitals, to be referred to hereafter as approximation AS1, with one where each configuration has its own set, approximation AS2.

2.2. HFR

In the HFR package (Cowan 1981), orbital bases are obtained for each configuration by solving for the spherically average atom the Hartree–Fock equations obtained by applying the variational principle to the configuration average energy. Relativistic corrections neglect the Breit terms listed in Eq. (3). Ab-initio eigenstates and eigenvalues are obtained and used to calculate A-values and wavelengths for each possible transition. Autoionization rates are calculated in a perturbation theory scheme where the radial functions of the initial and final states are optimized separately, and CI is accounted for only in the autoionizing state. Data sets computed with HFR are labelled HF1.

2.3. BPRM

The Breit–Pauli R-matrix package (Berrington et al. 1987; Seaton 1987) is based on the close-coupling approximation whereby the wavefunctions for states of an N-electron target and a colliding electron with total angular momentum and parity $J\pi$ are expanded in terms of the target eigenfunctions

$$\Psi^{J\pi} = \mathcal{A}\sum_i \chi_i \frac{F_i(r)}{r} + \sum_j c_j \Phi_j \ . \tag{5}$$

The functions χ_i are vector coupled products of the target eigenfunctions and the angular components of the incident-electron functions; $F_i(r)$ are the radial part of the continuum wavefunctions that describe the motion of the scattered electron, and $\mathcal{A}$ is an antisymmetrization operator. The functions Φ_j are bound-type functions of the total system constructed with target orbitals. Breit–Pauli relativistic corrections have been implemented in BPRM by Scott & Burke (1980) and Scott & Taylor (1982), but the inclusion of the two-body terms (see Eq. 3) is at present in progress. Auger and radiative dampings are taken into account through an optical potential (Robicheaux et al. 1995; Gorczyca & Badnell 1996, 2000a) where the resonance energy with respect to the threshold acquires an imaginary component.

In the present work, the N-electron targets are represented with all the fine structure levels within the $n = 2$ complex, and level energies are set to those obtained in approximation

AS2. Positions for states of the $(N+1)$-electron system are obtained from the peaks in the photoionization cross sections. This data set is referred to as RM1.

3. Energy levels and wavelengths

We have looked into several interactions that can influence the accuracy of the atomic data, namely CI, relativistic corrections, and CRE. We have found by calculation that configuration interaction from the $n = 3$ complex gives rise to small contribution that can be generally neglected. Computations are carried out in intermediate coupling with relativistic corrections even though the latter are small in particular for low ionization stages. Some effort is focused in characterizing CRE.

Energies calculated with approximations AS1, AS2, HF1, and RM1 for levels within the $n = 2$ complex of O ions are listed in Table 1. Since the accuracy of the transition data (e.g. wavelengths and gf-values) depends on the representations of both the lower (valence) and upper (K-vacancy) levels, detailed comparisons are carried out for each type. For the valence levels (see Table 2), a comparison of AS1 and AS2 reveals the importance of CRE which lower energies by as much as 20%. Since RM1 also neglects CRE, the best accord is with AS1: within 15% although the RM1 energies are on average lower by 4%. It may be noted that the RM1 calculation for O I has been performed in LS coupling due to the large size of the relativistic option. AS2 and HF1 agree to 5% and within 10% with the spectroscopic values (Moore 1998) which we find satisfactory.

Regarding K-vacancy levels, the energy differences of the approximations considered with respect to AS2 are plotted in Fig 1. The comparison with AS1 shows that, for species with a half-filled L shell or with greater electron occupancies ($6 \leq N \leq 8$ and $E < 544$ eV), CRE again lower energies but by amounts that increase with N: $\Delta E \equiv E(AS1) - E(AS2) <$ 0.7 eV for $N = 6$ to $\Delta E \approx 2.5$ eV for $N = 8$. On the other hand, for ions with a half-empty L shell or with lower occupancies ($2 \leq N \leq 5$ and $E > 544$ eV), level energies are raised by CRE particularly for $N = 3$ where $\Delta E \gtrsim -1.35$ eV. RM1 behaves, as expected, in a similar fashion to AS1, but some inconsistencies (e.g. lowered rather than raised levels) are present for $N < 6$ perhaps due to resolution problems in determining the position of narrow resonances in the photoionization curves. The agreement between the AS2 and HF1 energies is a sound ± 0.6 eV which sets a limit to the accuracy level that we can attain, and encourages us to adopt AS2 and HF1 as our working approximations.

AS2 and HF1 K-vacancy level energies are compared with experiment and other theoretical data in Table 3. It may be noted that there are no reported measurements for species

with $4 \leq N \leq 6$. HF1 level energies are within 0.5 eV of the spectroscopic values for $N \leq 3$ and the CI values by Charro et al. (2000) for $N = 2$ while AS2 is undesirably higher (0.9 eV) for the [1s]2p $^3P^o_1$ level in O VII. A convincing comparison with experiment for $N \geq 7$ is impeded by the scatter displayed in measurements which is well outside the reported error bars, but the photoionization measurements by Stolte et al. (1997) are 1 eV lower than HF1. The energy positions computed by Pradhan et al. (2003) with BPRM are noticeably higher than present results for $N > 4$, in particular for the B-like system ($N = 5$) where discrepancies as large as 5 eV are encountered. The values listed by McLaughlin & Kirby (1998) for O II ($N = 7$), which are also distinctively high ($\sim$ 3 eV), correspond to the CI target they prepared for the non-relativistic R-matrix calculation of the photoionization of O I. They contrast with those quoted for an equivalent target by Gorczyca & McLaughlin (2000b) which are in good agreement with Stolte et al. (1997). However, the values obtained by McLaughlin & Kirby (1998) for the [1s]2p^5 ^{3}P^o hole state in O I is in good agreement with AS2 and HF1.

CRE also have an impact on the transition wavelengths where, as depicted in Fig. 2, the comparison of AS1 and RM1 with AS2 indicates that in general CRE lead to increasingly longer wavelength for $N \geq 6$ ($\lambda > 23$ Å) and shorter for higher charge states. It may also be seen in Fig. 2 that wavelengths obtained with AS2 and HF1 agree to ± 0.02 Å setting again an accuracy bound. (AS2 and HF1 wavelengths are also listed in Table 4.) The present wavelengths are compared with experiment and other theoretical predictions in Table 5. For $N \leq 4$ present data, in particular HF1, agree with measurements and Vainshtein & Safranova (1978) to ± 0.02 Å; in this respect, for $2 < N \leq 4$ the values by Chen (1985, 1986) are somewhat long while those by Behar & Kahn (2002) are short, and for $N = 3$ the values by Pradhan et al. (2003) are long. For $5 \leq N \leq 6$ the outcome is less certain due to absence of laboratory measurements and inconsistencies in the computed values, e.g. the order of the upper levels in $N = 5$. For $N > 6$ the comparison with measurements seem to indicate that all theoretical results are slightly short although the agreement of HF1 is still within ~ 0.02 Å except for the transition from the ground level of O II and the measurement by Stolte et al. (1997) in O I which are just out (less than 0.05Å). It must be point out again the undesirable scatter of the experimental data for O I.

4. gf-values

In the following discussion of gf-values, the transitions involving the strongly mixed [1s]2p^4 ^{2}D$_{3/2}$ and ^{2}P$_{3/2}$ levels in O II are excluded due to extensive cancellation that result in completely unreliable data. Also the 1s^2 ^{1}S$_0$ $\rightarrow$ [1s]2p ^{3}P$^o_1$ intercombination transition in

O VII with a very small gf-value ($gf < 10^{-3}$) that would require a much greater effort to guarantee respectful accuracy.

A comparison of gf-values obtained with the AS1 and AS2 approximations shows that CRE are relatively unimportant, leading to differences much less than 10% except for transitions to the four [1s]2s2p ^{2}P^o relatively mixed levels of O VI where they jump up to $\sim$ 15%. In Fig. 3 we compare the AS2 and HF1 gf-values (also listed in Table 4) showing an agreement within 10% except for O I where the latter are consistently 25% higher. In a comparison of AS2 and HF1 f-values with other theoretical data sets in Table 6, it is found that those by Pradhan et al. (2003) are generally 20% smaller; however, an interesting point arises regarding the discrepancies between AS2 and HF1 where Pradhan et al. (2003) favors AS2 for O I and HF1 for the small f-value in O VI (see Table 6).

5. Radiative and Auger widths

The radiative width of the jth level is defined as

$$A_j = \sum_i A_{ji} \tag{6}$$

where A_{ji} is rate (partial width) for a downward ($j > i$) transition. It is found by calculation that CRE disturb the radiative widths of K-vacancy levels in the O isonuclear sequence by 10% or less (5% for $N > 5$) except when strong admixture occurs, namely for [1s]2p^4 ^{2}D$_{3/2}$ and ^{2}P$_{3/2}$ in O II and the four [1s]2s2p ^{2}P^o levels in O VI where differences are around 20%.

By contrast, as shown in Fig. 4, CRE reduce Auger rates by amounts that grow with N: from 10% for $N = 4$ ($\log A_a < 14$) up to 35% for $N = 8$; however, this trend is broken for $N = 3$ due to strong level mixing where the [1s]2s2p(^{3}P^o) ^{2}P^o_J are increased by a factor of 2 (not shown in Fig. 4) even though the [1s]2s2p(^{1}P^o) ^{2}P^o_J levels are hardly modified (less than 5%). The Auger widths obtained with HF1 for the former levels are $\sim$ 20% higher that AS2 while the rest, as shown in Fig. 4, are on average lower by 10%. With this outcome we would estimate an accuracy rating for the Auger rates at better than 20%. As further support for this assertion, in Table 7 we compare our branching ratios for KLL Auger transitions with other theoretical and experimental values. It may be seen that the AS1, AS2, and HF1 data are stable to better than 10%, and the accord with other data sets is for most cases better than 20%.

Radiative and Auger widths computed in approximations AS2 and HF1 are listed in Table 8.

6. Photoionization cross sections

High-energy photoionizations cross sections of O parent ions with electron occupancies of $3 \leq N \leq 8$ have been computed in approximation RM1; intermediate coupling has been used throughout except for O I because of computational size and negligible relativistic corrections. Following Gorczyca & Robicheaux (1999) and Gorczyca & McLaughlin (2000b), damping is taken into account in detail in order to bring forth the correct K threshold behavior. In Fig. 5 our cross sections are compared with those computed by Pradhan et al. (2003) with BPRM in the region near the $n = 2$ resonances; and by Reilman & Manson (1979) in a central field potential where it may be seen that, even though the background cross sections are in satisfactory accord, the positions and sharpness of the edges are discrepant. In the present approach, due to the astrophysical interest of both the $n = 2$ resonances and the edge region, the resonance structure is treated in a unified manner showing that a sharp K edge occurs only in the case of O VI due to the absence of spectator Auger (KLL) channels of the type

$$[1s]2p^{\mu}np \rightarrow 2p^{\mu-2}np + e^- \quad (7)$$

$$\rightarrow [2s]2p^{\mu-1}np + e^- \quad (8)$$

$$\rightarrow [2s]^2 2p^{\mu}np + e^- \ . \quad (9)$$

For the remaining ions KLL processes dominate over participator Auger (KLM) decay

$$[1s]2p^{\mu}np \rightarrow 2p^{\mu-1} + e^- \quad (10)$$

$$\rightarrow [2s]2p^{\mu} + e^- \quad (11)$$

causing edge smearing due to resonances with symmetric profiles of nearly constant width. Participator Auger decay, on the other hand, gives rise to the familiar Feschbach resonances—displayed by O VI in the region below the K threshold (see Fig. 5)—whose widths become narrower with n thus maintaining sharpness over the spectral head.

In order to elucidate further the interesting properties of K resonances, we analyze the experimental and theoretical predictions reported for the two $[1s]2p^4(^4P)np$ and $[1s]2p^4(^2P)np$ Rydberg series in O I that exhibit significant discrepancies. Regarding resonance positions, a stringent test is to compare quantum defects, μ, defined as

$$E = E_{\rm lim} - \frac{z}{(n-\mu)^2} \quad (12)$$

where $E_{\rm lim}$ is the series-limit energy in Rydbergs; $z \equiv Z - N + 1$ is the effective charge ($z = 1$ for O I); and n is the principal quantum number. In Fig. 6, the RM1 quantum defects for these two series are plotted relative to their respective series limits and compared with those obtained in photoionization measurements (Stolte et al. 1997) and the R-matrix

calculation of McLaughlin & Kirby (1998). Firstly, it may be seen that the experimental error bars grow sharply with n; hence greater accuracy for high n is obtained by quantum-defect extrapolation rather than actual measurement. Secondly, the agreement of experiment with RM1 is very good while that with McLaughlin & Kirby (1998), who used practically the same numerical method (R-matrix), is only a poor 40%. This outcome may be due to their neglect of damping effects or their choice of a Hartree–Fock basis for the 1s, 2s, and 2p orbitals which results in a deficient representation for the K-vacancy states. Since the R-matrix method employs a common set of target orbitals for both valence and K-vacancy states, we have found the most adequate orbital basis to be that optimized variationally with an energy sum comprising all the states in the target model. The importance of K-vacancy state representations has also been stressed by Gorczyca & McLaughlin (2000b). Thirdly, it is found that the RM1 quantum defects ($n \geq 3$) are hardly modified by small target-energy shifts prior to Hamiltonian diagonalization, a standard R-matrix procedure to enhance accuracy by using experimental thresholds; thus, the absolute energy positions of these resonances mostly depends on the actual position of their series limits. Moreover, as shown in Fig. 7, the huge and incorrect quantum-defect decline obtained for high n in McLaughlin & Kirby (1998) when using two different sets of experimental thresholds, namely those of Krause (1994) and Stolte et al. (1997), are not due, in our opinion, to the actual threshold-energy shifts but to resonance misidentifications: in such cases, $\mu(n+1) - \mu(n) \approx -1$ instead of approximately zero (see Fig. 7). The quantum-defect changes for $n \leq 6$ in McLaughlin & Kirby (1998) as thresholds are shifted are very small in accord with our mentioned finding. By contrast, the experimental quantum defects are sensitive to the series-limit positions. This can be appreciated in Fig. 7 when the quantum defects in the photoionization experiment of Menzel et al. (1996) are computed with the series limits by Krause (1994), on the one hand, and with those by Stolte et al. (1997) on the other, the latter resulting in unanimous agreement.

It is inferred from the above comparison that the energy positions obtained by Auger electron spectrometry (Krause 1994; Caldwell et al. 1994) for the $[1s]2p^4\ {}^4P$ and ${}^2P$ states of O II and listed in Table 3 should perhaps be scaled down by 0.4 eV. If this proposition is extended to the $[1s]2p^5\ {}^3P^o$ state of O I, then the measurements by Stolte et al. (1997) and Krause (1994) are brought to close agreement; the only remaining experimental discrepancy for the latter state would then be the measurement by Menzel et al. (1996) high by 1 eV. Furthermore, contrary to the $[1s]2p^4({}^4P)np\ {}^3P^o$ resonances of O I in our RM1 calculation, the absolute energy position of $[1s]2p^5\ {}^3P^o$ is insensitive to threshold-energy shifts. This is a consequence of its wavefunction being mostly represented by the second term of the close-coupling expansion (5). Therefore, a useful parameter in comparisons with experiment—in as much as it gives an indication of a balanced close-coupling expansion and experimental

consistency—is the energy interval between the lowest $n = 2$ and $n = 3$ resonances, $\Delta E(2,3)$ say. In Table 9, the RM1 $\Delta E(2,3)$ for the whole O isonuclear sequence are tabulated and compared with experimental and theoretical estimates. The 0.07 Ryd (1 eV) discrepancy in the $\Delta E(2,3)$ obtained from their measurements by Stolte et al. (1997) and Menzel et al. (1996) in O I ($N = 8$) denotes irregular data: since the positions for the (^{4}P)3p state differ by only 0.07 eV the issue is then the [1s]2p^5 ^{3}P°. The agreement of RM1 with Stolte et al. (1997) is very good; however, if the RM1 (^{4}P) threshold is improved by replacement with the experimental value at Halmiltonian diagonalization, then $\Delta E(2,3)$ reduces to 1.00. In other words, the introduction of experimental thresholds improves the positions of resonances with $n \geq 3$ relative to the ionization threshold but not those within $n = 2$, as previously mentioned. It may be appreciated in Table 9 that this finding is corroborated by the $\Delta E(2,3)$ resulting from the threshold-energy shifting in McLaughlin & Kirby (1998). It is also seen in Table 9 that for the O isonuclear sequence $\Delta E(2,3) \approx z$ for $N \geq 2$ and $\Delta E(2,3) \approx z+1$ for $N = 1$ if $\Delta E(2,3)$ is expressed in Ryd.

Regarding K-resonance widths in O I, from the Auger rates listed in Table 8 widths of 159 meV (AS2) and 163 meV (HF1) are obtained for [1s]2p^5 ^{3}P°. These are in good accord ($\sim$ 15%) with the measurements of 140 meV (Krause 1994; Menzel et al. 1996) and 142 eV (Stolte et al. 1997) and the theoretical estimates of 169 meV (Saha 1994) and 139 meV (Petrini & Araújo 1994). The value of 185.22 meV listed by McLaughlin & Kirby (1998), on the other hand, is somewhat high. The latter authors also predict for the [1s]2p^4(^{4}P)np ^{3}P° widths that decrease with n. As previously mentioned, the utter dominance of KLL Auger decay (see Eqs 7–9) gives rise to resonances of constant widths that have been confirmed with AS1 for $3 \leq n \leq 5$ to be at 103 meV and with a KLM branching ratio of 5 parts in 1000 or less.

7. Opacities

In order to evaluate the accuracy of the present calculations, all the previously discused atomic data were included in the modelling code XSTAR (Kallman & Bautista 2001). The opacities for six different ionization parameters ($0.001 \leq \xi \leq 10$) were obtained with a simple model including the following values: gas density of 10^{12} cm^{-3}, X-ray luminosity source of 10^{44} erg/s and the solar abundances for H, He and O elements. Since the density remains constant, the well known (Tarter et al. 1969) form for the ionization parameter is implemented:

$$\xi = L/nR^2 \tag{13}$$

being L the luminosity of the source, n the density of the gas and R the distance to the emiting source. Thus, the monocromatic opacities are calculated assuming that ionization and heating are principally due to an external source of continuum photons. In Fig. (8) the results for each $log(\xi)$ are plotted in the energy range of $400 - 800$ eV, where the K edges for the different oxygen ions appears according to the ionization parameter.

The top-left plot ($log(\xi) = -3$) represents the opacity for a low-ionized plasma, where a sharp K edge appears near to the 545 eV region, due to O I as well as the resonance structure near $530 - 540$ eV that correspond to the Kα resonances of O I and O II. In the second graph in the left panel for $log(\xi) = -2$, the O II K edge begins to be strong in the ~ 565 eV region, while in the bottom-left plot ($log(\xi) = -1.5$) this edge disappears when the O III and O IV K edges are evident at ~ 600 eV and ~ 630 eV respectively. For the top-right plot which correspond to $log(\xi) = -1$, the O IV contribution continues been strong, but in this opacity the O V K edge is predominant at ~ 665 eV. The O V edge is also the most important feature in the $log(\xi) = 0$ case, where the ionization of the gas is high enough to allow the participation of O VI in the opacity, as can be seen in the small K edge near to 700 eV. The last plot (bottom-right) reproduces the case of a highly ionized gas with $log(\xi) = 1$, and thc opacity is dominated by the O V, O VI and O VII K edges in the high energy region. In these stages, the Kβ and higher resonances apper as strong absorption features causing a smeared K edge in the opacities, the opposite characteristic of the low-ionized opacities.

This behavior at the two extremes of ionization parameter is similar to that reported for the iron isonuclear sequence (Palmeri et al. 2002). An important difference with iron is that the oxygen opacities show important absoption features the region near the K edge, because the L-shell in the neutral oxygen ions is not completly full. As a result there are stronger absorption channels open in the oxygen case.

8. Discussion and conclusions

Extensive computations of the atomic data required for the spectral modelling of K-shell photoabsorption of oxygen ions have been carried out in a multi-code approach. This method has proven to be—as in a previous systematic treatment of the Fe isonuclear sequence (Bautista et al. 2003; Palmeri et al. 2003a,b; Bautista et al. 2004; Mendoza et al. 2004)—effective in sizing up the relevant interactions and in obtaining estimates of accuracy ratings, the latter often overlooked in theoretical work. Inter-complex CI and relativistic corrections are found to be small, but CRE are shown to be conspicuous in most processes involving K-vacancy states. The inclusion of CRE in ion representations is therefore compelling which in practice is managed (e.g. in the HFR and AUTOSTRUCTURE codes) by considering non-

orthogonal orbital bases for K-vacancy and valence states; otherwise (e.g. BPRM) orthogonal orbital bases are optimized by minimizing energy sums that span both type of states.

By considering several approximations and comparing with reported experimental and theoretical data, the present level energies and wavelength for O ions with electron occupancies $N \leq 4$ are estimated to be accurate to within 0.5 eV and 0.02 Å, respectively. For ions with $N > 4$, the absence of measurements in particular for $5 \leq N \leq 6$, the wide experimental scatter for $N > 6$, and discrepancies among theoretical data sets make the estimate of reliable accuracy ratings less certain. It is found that for $N > 4$ our level energies (wavelengths) are probably somewhat high (short) by up to 1.5 eV (0.05 Å) in neutral oxygen. Our best results are from approximation HF1.

The radiative data (gf-values and total widths) computed with approximations AS2 and HF1 are expected to be accurate to 10% except in O I where the rating is not better than 25% and in transitions involving strongly mixed levels, namely the [1s]2p^4 ^{2}D$_{3/2}$ and ^{2}P$_{3/2}$ levels in O II and to a lesser extent the four [1s]2s2p ^{2}P^o_J levels in O VI, where it is unbound. Admixture in the latter levels also affect Auger rates which otherwise are expected to be accurate to 20%. The complete and ranked set of radiative and Auger data for transitions involving K-vacancy levels in O ions is one of the main contributions of the present work.

A second contribution are the high-energy photoabsorption cross sections for ions with $N > 3$ that depict in detail the resonance structure of the K edge. Such structure has been shown to be dominated by KLL damping (often neglected in previous work) which gives the edge a blunt imprint with arguably diagnostic potential. A comparison with the experimental K resonance positions in O I results in conclusive statements about the importance of R-matrix computations with well balanced close-coupling expansions, i.e. where both terms of expression (5) are separately convergent. In this respect, the accuracy of the energy interval between the $n = 2$ and $n = 3$ components of a K resonance series gives a measure of the close-coupling balance, and for the O isonuclear sequence, this energy interval when expressed in Ryd has been shown to be close to the effective charge, $z \equiv Z - N + 1$, for members with $N \geq 2$ and near $z + 1$ for $N = 1$. This finding could be exploited in spectral identification.

As a follow-on to the present work, we intend to treat with the same systematic methodology the Ne isonuclear sequence and then other sequences of astrophysical interest (Mg, Si, S, Ar, and Ca), always bearing in mind the scanty availability of laboratory measurements which as shown in the present work are unreplaceable requisites in theoretical fine-tuning.

MAB acknowledges partial support from FONACIT, Venezuela, under contract No. S1-20011000912. TWG was supported in part by the NASA Astronomy and Physics Research

and Analysis Program.

REFERENCES

Badnell, N. R. 1986, J. Phys. B, 19, 3827

Badnell, N. R. 1997, J. Phys. B, 30, 1

Bautista, M. A., Mendoza, C., Kallman, T. R., & Palmeri, P. 2003, A&A, 403, 339

Bautista, M. A., Mendoza, C., Kallman, T. R., & Palmeri, P. 2004, A&A, 418, 1171

Behar, E., et al. 2003, ApJ, 598, 232

Behar, E., & Kahn, S. M. 2002, in NASA Laboratory Astrophysics Workshop, ed. F. Salama (NASA/CP-2002-21186), p23

Beiersdorfer, P., et al. 2003, Science, 300, 1558

Berrington, K. A., Burke, P. G., Butler, K., Seaton, M. J., Storey, P. J., Taylor, K. T., & Yu Yan. 1987, J. Phys. B, 20, 6379

Cagnoni, N., Nicastro, F., Maraschi, L., Treves, A., & Tavecchio F. 2004, ApJ, 603, 449

Caldwell, C. D., & Krause, M. O. 1993, Phys. Rev. A, 47, R759

Caldwell, C. D., Schaphorst, S. J., Krause, M. O., & Jiménez-Mier, J. 1994, J. Electron. Spectrosc. Relat. Phenom., 67, 243

Charro, E., Bell, K. L., Martin, I., & Hibbert, A. 2000, MNRAS, 313, 247

Chen, M. H. 1985, Phys. Rev. A, 31, 1449

Chen, M. H. 1986, At. Data Nucl. Data Tables, 34,301

Cowan, R. D. 1981, The Theory of Atomic Spectra and Structure, (Berkeley, CA: University of California Press)

de Vries, C. P., den Herder, J. W., Kaastra, J. S., Paerels, F. B., den Boggenden, A. J., & Rasmussen, A. P. 2003, A&A, 404, 959

Eissner, W., Jones, M., & Nussbaumer, H. 1974, Comput. Phys., Commun., 8, 270

Engström, L., & Litzén, U. 1995, J. Phys. B, 28, 2565

Gorczyca, T. W., & Badnell, N. R. 1996, J. Phys. B, 29, L283

Gorczyca, T. W., & Badnell, N. R. 2000a, J. Phys. B, 33, 2511

Gorczyca, T. W., & McLaughlin, B. M. 2000b, J. Phys. B, 33, L859

Gorczyca, T. W., & Robicheaux, F. 1999, Phys. Rev. A, 60, 1216

Juett, A. M., Schulz, N. S., & Chakrabartty, D. 2004, ApJ, 612, 308

Kallman, T., & Bautista, M. 2001, ApJS, 133, 221

Kallman, T. R., Palmeri, P., Bautista, M. A., Mendoza, C., & Krolik, J. H. 2004, ApJS, in press

Kawatsura, et al. 2002, J. Phys. B, 35, 4147

Krause, M. O. 1994, Nucl. Instrum. Meth. Phys. Res. B, 87, 178

Lee, J. C., Ogle, P. M., Canizares, C. R., Marshall, H. L., Schulz, N. S., Morales, R., Fabian, A. C., & Iwasawa, K. 2001, ApJ, 554, L13

Loeb, A. 2003, Phys. Rev. Lett., 91, 071103

McLaughlin, B. M., & Kirby, K. P. 1998, J. Phys. B, 31, 4991

Mendoza, C., Kallman, T. R., Bautista, M. A., & Palmeri, P. 2004, A&A, 414, 377

Menzel, A., Benzaid, S., Krause, M. O., Caldwell, C. D., Hergenhahn, U., & Bissen, M. 1996, Phys. Rev. A, 54, R991

Moore, C. E. 1998, Tables of spectra of hydrogen, carbon, nitrogen, and oxygen atoms and ions, ed. J. W. Gallagher (Boca Raton, FL: CRC Press)

Page, M. J., Soria, R., Wu, K., Mason, K. O., Cordova, F. A., & Priedhorsky, W. C. 2003, MNRAS, 345, 639

Palmeri, P., Mendoza, C., Kallman, T. R., & Bautista, M. A. 2002, ApJ, 577, L119

Palmeri, P., Mendoza, C., Kallman, T. R., & Bautista, M. A. 2003a, A&A, 403, 1175

Palmeri, P., Mendoza, C., Kallman, T. R., Bautista, M. A. & Meléndez, M. 2003b, A&A, 410, 359

Petrini, D., & Araújo, F. X. 1994, å, 282, 315

Pradhan, A. K., Chen, G. X., Delahaye, F., Nahar, S. N., & Oelgoetz, J. 2003, MNRAS, 341, 1268

Reilman, R. F., & Manson, S. T. 1979, ApJS, 40, 815

Robicheaux, F., Gorczyca. T. W., Pindzola, M. S., & Badnell, N. R. 1995, Phys. Rev. A, 32, 1319

Saha, H. P. 1994, Phys. Rev. A, 49, 894

Sako, M. 2003, ApJ, 594, 1108

Sako, M., et al. 2003, ApJ, 596, 114

Saraph, H. E. 1987, Comput. Phyts. Commun., 46, 107

Schmidt, M., Beiersdorfer, P., Chen, H., Thorn, D. B., Träbert, E., & Behar, E. 2004, ApJ, 604, 562

Schulz, N. S., Cul, W., Canizares, C. R., Marshall, H. L., Lee, J. C., Miller, J. M., & Lewin, W. H. G. 2002, ApJ, 565, 1141

Scott, N. S., & Burke, P. G. 1980, J. Phys. B, 13, 4299

Scott, N. S., & Taylor, K. T. 1982, Comput. Phys. Commun., 25, 347

Seaton, M. J. 1987, J. Phys. B, 20, 6363

Steenbrugge, K. C., Kaastra, J. S., de Vries, C. P., & Edelson, R. 2003, A&A, 402, 477

Stolte, W. C., et al. 1997, J. Phys. B, 30, 4489

Vainshtein, L. A., & Safranova, U. I. 1971, Soviet Astron.-AJ, 15, 175

Vainshtein, L. A., & Safranova, U. I. 1978, At. Data Nucl. Data Tables, 21, 49

Tarter, C.B., Tucker, W. and Salpeter, E. 1969, ApJ, 156, 943

Fig. 1.— Energy differences for K-vacancy levels in the O isonuclear sequence computed with approximation AS2 and those with AS1 (open circles), HF1 (solid circles) and RM1 (solid triangles). Differences with AS1 and RM1 are due mainly to CRE. The agreement between AS2 and HF1 is within ± 0.5 eV.

Fig. 2.— Wavelength differences for Kα transitions in the O isoelectronic sequence computed with approximation AS2 and those with AS1 (open circles), HF1 (solid circles), and RM1 (solid triangles). The agreement between AS2 and HF1 is within ± 0.02 Å.

Fig. 3.— Comparison of gf-values for Kα transitions in O ions computed with approximations AS2 and HF1. It may be seen that, while the agreement for most transitions is within 10%, the HF1 gf-values for O I are consistently larger by 25%.

Fig. 4.— Comparison of Auger widths (s^{-1}) for K-vacancy levels in O ions computed with approximations AS2 with those of AS1 (filled circles) and HF1 (open circles). Differences between AS1 and AS2 (as large as 35%) are due to CRE. It may also be seen that HF1 are on average 10% lower than AS2.

Fig. 5.— High-energy photoionization cross sections of O ions showing the structure of the K edge. Black curve — RM1; red curve — Pradhan et al. (2003); green curve — Reilman & Manson (1979).

Fig. 6.— Quantum defects for the (a) $[1s]2p^4(^4P)np\ ^3P^o$ and (b) $[1s]2p^4(^2P)np\ ^3P^o$ ($3 \leq n \leq 6$) resonance series of O I plotted relative to the respective threshold energy. Circles — present RM1 results. Filled circles — experiment of Stolte et al. (1997). Filled triangles — R-matrix data by McLaughlin & Kirby (1998).

Fig. 7.— Quantum defects for the (a) $[1s]2p^4(^4P)np\ ^3P^o$ and (b) $[1s]2p^4(^2P)np\ ^3P^o$ ($3 \leq n \leq 10$) resonance series of O I plotted relative to the respective threshold energy. Circles — experiment of Krause (1994) and Menzel et al. (1996). Filled circles — experiment of Stolte et al. (1997). Triangles — R-matrix quantum defects of McLaughlin & Kirby (1998) relative to the experimental thresholds of Krause (1994). Filled triangles — R-matrix quantum defects of McLaughlin & Kirby (1998) relative to the experimental threshold by Stolte et al. (1997).

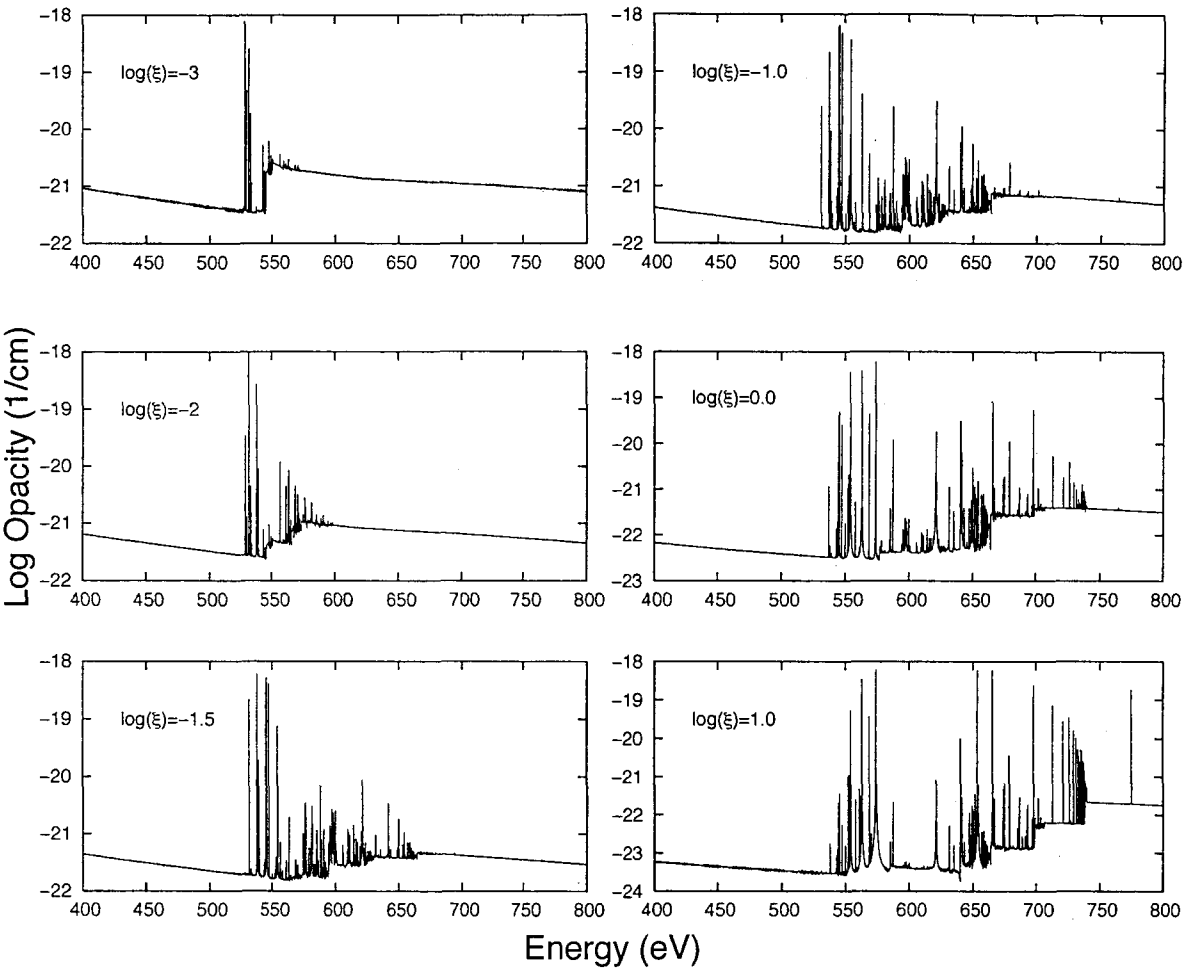

Fig. 8.— Opacities for photoionized gas with respect to the photon energy in the K edge region for ionization parameters $-3 \leq log(\xi) \leq 1$.

Table 1. Calculated energies (eV) for valence and K-vacancy levels in O ions

N	i	Level	AS1	AS2	HF1	RM1	N	i	Level	AS1	AS2	HF1	RM1
2	1	$1s^2\ ^1S_0$	0.000	0.000	0.000		7	1	$2p^3\ ^4S^o_{3/2}$	0.000	0.000	0.000	0.000
2	2	$[1s]2p\ ^3P^o_1$	566.9	567.7	568.1		7	2	$2p^3\ ^2D^o_{5/2}$	3.972	3.711	3.770	3.615
2	3	$[1s]2p\ ^1P^o_1$	572.5	573.5	573.7		7	3	$2p^3\ ^2D^o_{3/2}$	3.975	3.714	3.770	3.614
3	1	$2s\ ^2S_{1/2}$	0.000	0.000	0.000	0.000	7	4	$2p^3\ ^2P^o_{3/2}$	5.393	5.064	5.131	5.655
3	2	$[1s]2s2p\ ^2P^o_{1/2}$	561.7	563.0	562.7	563.4	7	5	$2p^3\ ^2P^o_{1/2}$	5.395	5.066	5.131	5.654
3	3	$[1s]2s2p\ ^2P^o_{3/2}$	561.7	563.1	562.7	563.4	7	6	$[1s]2p^4\ ^4P_{5/2}$	533.2	531.8	531.7	532.5
3	4	$[1s]2s2p\ ^2P^o_{1/2}$	567.4	568.6	568.0	568.0	7	7	$[1s]2p^4\ ^4P_{3/2}$	533.3	531.9	531.7	532.5
3	5	$[1s]2s2p\ ^2P^o_{3/2}$	567.4	568.6	568.1	568.0	7	8	$[1s]2p^4\ ^4P_{1/2}$	533.3	531.9	531.7	532.5
4	1	$2s^2\ ^1S_0$	0.000	0.000	0.000	0.000	7	9	$[1s]2p^4\ ^2D_{5/2}$	537.3	536.1	536.1	537.0
4	2	$[1s]2p\ ^1P^o_1$	554.2	554.5	554.4	554.1	7	10	$[1s]2p^4\ ^2D_{3/2}$	537.3	536.1	536.1	537.0
5	1	$2p\ ^2P^o_{1/2}$	0.000	0.000	0.000	0.000	7	11	$[1s]2p^4\ ^2P_{3/2}$	537.4	536.2	536.3	537.5
5	2	$2p\ ^2P^o_{3/2}$	0.057	0.049	0.047	0.047	7	12	$[1s]2p^4\ ^2P_{1/2}$	537.4	536.2	536.3	537.5
5	3	$[1s]2p^2\ ^2D_{5/2}$	544.1	544.6	544.3	544.4	7	13	$[1s]2p^4\ ^2S_{1/2}$	539.3	538.4	538.3	540.4
5	4	$[1s]2p^2\ ^2D_{3/2}$	544.1	544.6	544.3	544.4	8	1	$2p^4\ ^3P_2$	0.000	0.000	0.000	0.000
5	5	$[1s]2p^2\ ^2P_{1/2}$	544.8	545.2	545.0	545.3	8	2	$2p^4\ ^3P_1$	0.023	0.020	0.018	0.000
5	6	$[1s]2p^2\ ^2P_{3/2}$	544.8	545.3	545.0	545.3	8	3	$2p^4\ ^3P_0$	0.033	0.029	0.027	0.000
5	7	$[1s]2p^2\ ^2S_{1/2}$	546.5	547.1	547.3	548.2	8	4	$2p^4\ ^1D_2$	2.353	2.181	2.200	2.149
6	1	$2p^2\ ^3P_0$	0.000	0.000	0.000	0.000	8	5	$2p^4\ ^1S_0$	4.244	3.975	3.979	4.833
6	2	$2p^2\ ^3P_1$	0.016	0.014	0.014	0.014	8	6	$[1s]2p^5\ ^3P^o_2$	531.4	528.8	528.2	529.7
6	3	$2p^2\ ^3P_2$	0.044	0.037	0.040	0.040	8	7	$[1s]2p^5\ ^3P^o_1$	531.4	528.8	528.2	529.7
6	4	$2p^2\ ^1D_2$	2.958	2.750	2.848	2.711	8	8	$[1s]2p^5\ ^3P^o_0$	531.4	528.9	528.3	529.7
6	5	$2p^2\ ^1S_0$	5.390	5.000	5.237	6.089	8	9	$[1s]2p^5\ ^1P^o_1$	533.5	531.2	530.8	532.7
6	6	$[1s]2p^3\ ^3D^o_3$	537.5	536.9	537.0	536.9							
6	7	$[1s]2p^3\ ^3D^o_2$	537.5	536.9	537.0	536.9							
6	8	$[1s]2p^3\ ^3D^o_1$	537.5	536.9	537.0	537.0							
6	9	$[1s]2p^3\ ^3S^o_1$	538.0	537.4	537.7	538.0							
6	10	$[1s]2p^3\ ^3P^o_2$	538.9	538.4	538.6	539.4							
6	11	$[1s]2p^3\ ^3P^o_1$	538.9	538.5	538.7	539.4							
6	12	$[1s]2p^3\ ^3P^o_0$	538.9	538.5	538.7	539.4							
6	13	$[1s]2p^3\ ^1D^o_2$	540.8	540.3	540.6	540.7							
6	14	$[1s]2p^3\ ^1P^o_1$	542.2	541.9	542.2	543.1							

Table 2. Comparison of valence-level energies (eV)

N	Level	Expt[a]	AS1	AS2	HF1	RM1
5	$2p\ ^2P^o_{1/2}$	0.000	0.000	0.000	0.000	0.000
5	$2p\ ^2P^o_{3/2}$	0.048	0.057	0.049	0.047	0.047
6	$2p^2\ ^3P_0$	0.000	0.000	0.000	0.000	0.000
6	$2p^2\ ^3P_1$	0.014	0.016	0.014	0.014	0.014
6	$2p^2\ ^3P_2$	0.038	0.044	0.037	0.040	0.040
6	$2p^2\ ^1D_2$	2.514	2.958	2.750	2.848	2.711
6	$2p^2\ ^1S_0$	5.354	5.390	5.000	5.237	6.089
7	$2p^3\ ^4S^o_{3/2}$	0.000	0.000	0.000	0.000	0.000
7	$2p^3\ ^2D^o_{5/2}$	3.324	3.972	3.711	3.770	3.615
7	$2p^3\ ^2D^o_{3/2}$	3.327	3.975	3.714	3.770	3.614
7	$2p^3\ ^2P^o_{3/2}$	5.017	5.393	5.064	5.131	5.655
7	$2p^3\ ^2P^o_{1/2}$	5.018	5.395	5.066	5.131	5.654
8	$2p^4\ ^3P_2$	0.000	0.000	0.000	0.000	0.000
8	$2p^4\ ^3P_1$	0.020	0.023	0.020	0.018	0.000
8	$2p^4\ ^3P_0$	0.028	0.033	0.029	0.027	0.000
8	$2p^4\ ^1D_2$	1.967	2.353	2.181	2.200	2.149
8	$2p^4\ ^1S_0$	4.190	4.244	3.975	3.979	4.833

[a]Spectroscopic tables (Moore 1998)

Table 3. Comparison of K-vacancy level energies (eV)

N	State	AS2	HF1	Expt	Theory
2	[1s]2p $^3P^o_1$	567.7	568.1	568.6[a]	568.2[e]
2	[1s]2p $^1P^o_1$	573.5	573.7	574.0[a]	573.6[e]
3	[1s]2s2p($^3P^o$) $^2P^o$	563.1	562.7	562.6[a]	562.3[f]
3	[1s]2s2p($^1P^o$) $^2P^o$	568.6	568.1	568.2[a]	567.0[f]
4	[1s]2p $^1P^o_1$	554.5	554.4		554.6[f]
					553.15[g]
5	[1s]2p^2 $^2D_{3/2}$	544.6	544.3		545.8[f]
5	[1s]2p^2 ^2P	545.3	545.0		547.0[f]
5	[1s]2p^2 $^2S_{1/2}$	547.1	547.3		552.1[f]
6	[1s]2p^3 $^3D^o_1$	536.9	537.0		537.2[f]
6	[1s]2p^3 $^3S^o_1$	537.4	537.7		538.6[f]
6	[1s]2p^3 $^3P^o_1$	538.5	538.7		540.7[f]
7	[1s]2p^4 ^4P	531.9	531.7	530.8(3)[b]	532.9[f]
				530.42(4)[c]	531.0[h]
					534.1[i]
7	[1s]2p^4 ^2D	536.1	536.1		535.3[h]
					538.7[i]
7	[1s]2p^4 ^2P	536.2	536.3	535.7(3)[b]	535.9[h]
				535.24(4)[c]	539.2[i]
7	[1s]2p^4 ^2S	538.4	538.3		538.1[h]
					542.9[i]
8	[1s]2p^5 $^3P^o$	528.8	528.2	527.2(3)[b]	528.8[f]
				526.79(4)[c]	528.22[i]
				527.85(10)[d]	528.33[i]

[a]Spectroscopic tables (Moore 1998)

[b]Auger electron spectrometry (Krause 1994; Caldwell et al. 1994)

[c]Photoionization experiment (Stolte et al. 1997)

[d]Photoabsorption measurements (Menzel et al. 1996)

[e]Non-relativistic CI calculation (Charro et al. 2000)

[f]*R*-matrix calculation by Pradhan et al. (2003)

[g]Multiconfiguration Dirac–Fock calculation by Chen (1985)

[h]*R*-matrix calculation (Gorczyca & McLaughlin 2000b)

[i]*R*-matrix calculation (McLaughlin & Kirby 1998)

Table 4. Calculated wavelengths and gf-values for Kα transitions

			AS2		HF1					AS2		HF1	
N	i	j	λ (Å)	gf_{ij}	λ (Å)	gf_{ij}	N	i	j	λ (Å)	gf_{ij}	λ (Å)	gf_{ij}
2	1	2	21.84	1.22E−4	21.82	7.35E−5	6	4	13	23.06	1.35E+0	23.06	1.35E+0
2	1	3	21.62	8.27E−1	21.61	7.96E−1	6	4	14	23.00	5.09E−1	22.99	4.98E−1
3	1	2	22.02	4.93E−1	22.04	4.37E−1	6	5	14	23.09	3.37E−1	23.09	3.41E−1
3	1	3	22.02	9.95E−1	22.03	8.81E−1	7	1	6	23.31	4.24E−1	23.32	4.56E−1
3	1	4	21.80	4.53E−2	21.83	4.40E−2	7	1	7	23.31	2.83E−1	23.32	3.04E−1
3	1	5	21.80	8.23E−2	21.83	8.09E−2	7	1	8	23.31	1.41E−1	23.32	1.52E−1
4	1	2	22.36	7.08E−1	22.37	6.52E−1	7	2	9	23.29	6.22E−1	23.29	6.70E−1
5	1	4	22.77	3.53E−1	22.78	3.33E−1	7	2	10	23.29	1.00E−1	23.29	1.45E−2
5	1	5	22.74	4.36E−1	22.75	4.09E−1	7	2	11	23.29	6.72E−1	23.28	8.18E−1
5	1	6	22.74	1.89E−1	22.75	1.80E−1	7	3	9	23.29	4.09E−2	23.29	4.43E−2
5	1	7	22.66	7.15E−2	22.65	6.67E−2	7	3	10	23.29	4.76E−1	23.29	4.74E−1
5	2	3	22.77	5.90E−1	22.78	5.61E−1	7	3	11	23.29	1.48E−2	23.28	5.42E−2
5	2	4	22.77	4.21E−2	22.78	4.24E−2	7	3	12	23.29	3.98E−1	23.28	4.30E−1
5	2	5	22.74	2.06E−1	22.75	1.95E−1	7	4	9	23.35	2.00E−1	23.35	2.19E−1
5	2	6	22.74	1.09E+0	22.75	1.03E+0	7	4	10	23.35	2.04E−1	23.35	4.41E−2
5	2	7	22.66	1.68E−1	22.66	1.52E−1	7	4	11	23.35	1.66E−1	23.34	3.61E−1
6	1	8	23.09	1.41E−1	23.09	1.42E−1	7	4	12	23.34	7.48E−2	23.34	8.09E−2
6	1	9	23.07	1.30E−1	23.06	1.30E−1	7	4	13	23.25	2.12E−1	23.25	2.29E−1
6	1	11	23.03	8.40E−2	23.02	8.18E−2	7	5	10	23.35	1.38E−2	23.35	9.82E−2
6	2	7	23.09	3.17E−1	23.09	3.18E−1	7	5	11	23.35	1.67E−1	23.34	1.00E−1
6	2	8	23.09	1.00E−1	23.09	9.95E−2	7	5	12	23.34	1.46E−1	23.34	1.61E−1
6	2	9	23.07	3.82E−1	23.06	3.82E−1	7	5	13	23.25	1.01E−1	23.25	1.08E−1
6	2	10	23.03	1.07E−1	23.02	1.05E−1	8	1	6	23.45	4.31E−1	23.47	5.25E−1
6	2	11	23.03	6.52E−2	23.02	6.31E−2	8	1	7	23.44	1.44E−1	23.47	1.75E−1
6	2	12	23.03	9.31E−2	23.02	9.12E−2	8	2	6	23.45	1.44E−1	23.47	1.80E−1
6	3	6	23.10	5.75E−1	23.09	5.77E−1	8	2	7	23.45	8.61E−2	23.47	1.08E−1
6	3	7	23.09	9.36E−2	23.09	9.44E−2	8	2	8	23.44	1.15E−1	23.47	1.44E−1
6	3	8	23.09	5.77E−3	23.09	6.05E−3	8	3	7	23.45	1.15E−1	23.47	1.44E−1
6	3	9	23.07	6.11E−1	23.06	6.08E−1	8	4	9	23.44	6.28E−1	23.45	7.85E−1
6	3	10	23.03	3.58E−1	23.02	3.51E−1	8	5	9	23.52	1.05E−1	23.53	1.32E−1
6	3	11	23.03	1.31E−1	23.02	1.29E−1							

Table 5. Wavelength (Å) comparison for Kα transitions

N	i	j	AS2	HF1	Expt	Other theory
2	$1s^2\ ^1S_0$	$[1s]2p\ ^3P^o_1$	21.84	21.82	21.807[a]	21.84[i], 21.84[j]
	$1s^2\ ^1S_0$	$[1s]2p\ ^1P^o_1$	21.62	21.61	21.6020(3)[b]	21.60[i]
3	$2s\ ^2S$	$[1s]2s2p(^3P^o)\ ^2P^o$	22.02	22.03	22.038[a], 22.01(1)[c], 22.0194(16)[d]	22.02[i], 22.06[j], 22.05[k], 22.00[l]
	$2s\ ^2S$	$[1s]2s2p(^1P^o)\ ^2P^o$	21.80	21.83	21.82[a]	21.84[j],21.87[k], 21.79[l]
4	$2s^2\ ^1S$	$[1s]2p\ ^1P^o$	22.36	22.37	22.374(3)[d]	22.38[i], 22.41[j], 22.35[k], 22.33[l]
5	$2p\ ^2P^o_{1/2}$	$[1s]2p^2\ ^2D_{3/2}$	22.77	22.78	22.74(2)[c]	22.73[k], 22.73[l]
	$2p\ ^2P^o_{1/2}$	$[1s]2p^2\ ^2P$	22.74	22.75		22.67[k], 22.78[l]
	$2p\ ^2P^o_{1/2}$	$[1s]2p^2\ ^2S_{1/2}$	22.66	22.65		22.67[k], 22.73[l]
6	$2p^2\ ^3P_0$	$[1s]2p^3\ ^3D^o_1$	23.09	23.09	23.17(1)[c]	23.08[k], 23.11[l]
	$2p^2\ ^3P_0$	$[1s]2p^3\ ^3S^o_1$	23.07	23.06	23.00(1)[c]	23.02[k], 23.05[l]
	$2p^2\ ^3P_0$	$[1s]2p^3\ ^3P^o_1$	23.03	23.02		22.93[k], 22.98[l]
7	$2p^3\ ^4S^o$	$[1s]2p^4\ ^4P$	23.31	23.32	23.36(1)[e]	23.27[k], 23.30[l]
	$2p^3\ ^2D^o$	$[1s]2p^4\ ^2P$	23.29	23.28	23.29(1)[e]	
	$2p^3\ ^2P^o$	$[1s]2p^4\ ^2P$	23.35	23.34	23.36(1)[e]	
8	$2p^4\ ^3P$	$[1s]2p^5\ ^3P^o$	23.45	23.47	23.51(3)[e], 23.489(5)[f], 23.536(2)[g] 23.508(3)[h]	23.45[k]

[a]Spectroscopic tables (Moore 1998)

[b]Spectroscopic measurements (Engström & Litzén 1995)

[c]Spectroscopy of NGC 5548 (Steenbrugge et al. 2003)

[d]Electron beam ion trap measurements (Schmidt et al. 2004)

[e]Auger electron spectrometry (Krause 1994; Caldwell et al. 1994)

[f]Photoabsorption measurements (Menzel et al. 1996)

[g]Photoionization experiment (Stolte et al. 1997)

[h]ISM observations (Juett et al. 2004)

[i]1/Z expansion method (Vainshtein & Safranova 1971, 1978)

[j]Multiconfiguration Dirac–Fock calculation (Chen 1985, 1986)

[k]R-matrix calculation (Pradhan et al. 2003)

[l]HULLAC calculation (Behar & Kahn 2002)

Table 6. Comparison of theoretical f-values for Kα transitions

N	i	j	AS2	HF1	RM2[a]
3	$2s\ ^2S$	$[1s]2s2p(^3P^o)\ ^2P^o$	0.744	0.659	0.576
3	$2s\ ^2S$	$[1s]2s2p(^1P^o)\ ^2P^o$	0.077	0.062	0.061
4	$2s^2\ ^1S$	$[1s]2p\ ^1P^o$	0.708	0.652	0.565
5	$2p\ ^2P^o_{1/2}$	$[1s]2p^2\ ^2D_{3/2}$	0.177	0.167	0.132
5	$2p\ ^2P^o_{1/2}$	$[1s]2p^2\ ^2P$	0.313	0.295	0.252
5	$2p\ ^2P^o_{1/2}$	$[1s]2p^2\ ^2S_{1/2}$	0.036	0.033	0.027
6	$2p^2\ ^3P_0$	$[1s]2p^3\ ^3D^o_1$	0.141	0.142	0.119
6	$2p^2\ ^3P_0$	$[1s]2p^3\ ^3S^o_1$	0.130	0.130	0.102
6	$2p^2\ ^3P_0$	$[1s]2p^3\ ^3P^o_1$	0.084	0.082	0.067
7	$2p^3\ ^4S^o_{3/2}$	$[1s]2p^4\ ^4P$	0.212	0.228	0.184
8	$2p^4\ ^3P_2$	$[1s]2p^5\ ^3P$	0.115	0.140	0.113

[a] R-matrix data by Pradhan et al. (2003)

Table 7. Comparison of branching ratios for KLL Auger transitions

N	i	j	AS1	AS2	HF1	Expt[a]	MCDF[b]	CC[c]
7	$[1s]2p^4\ ^4P$	$2p^2$	0.42	0.42	0.43	0.55(13)	0.36	0.43
		$[2s]2p^3$	0.41	0.40	0.40	0.33(3)	0.46	0.42
		$[2s^2]2p^4$	0.17	0.18	0.18	0.12(2)	0.18	0.15
7	$[1s]2p^4\ ^2P$	$2p^2$	0.53	0.53	0.51	0.53(9)	0.45	0.47
		$[2s]2p^3$	0.27	0.27	0.28	0.28(4)	0.31	0.28
		$[2s^2]2p^4$	0.20	0.20	0.21	0.19(3)	0.24	0.25
8	$[1s]2p^5\ ^3P^o$	$2p^3$	0.53	0.51	0.55	0.602		
		$[2s]2p^4$	0.35	0.35	0.32	0.30		
		$[2s^2]2p^5$	0.12	0.14	0.13	0.094		

[a] Auger electron spectrometry (Caldwell & Krause 1993; Caldwell et al. 1994)

[b] MCDF calculation by M. H. Chen as quoted in Caldwell et al. (1994)

[c] Close-coupling calculation (Petrini & Araújo 1994)

Table 8. Calculated radiative and Auger widths for K-vacancy levels

			AS2		HF1	
N	i	Level	A_r (s^{-1})	A_a (s^{-1})	A_r (s^{-1})	A_a (s^{-1})
2	2	[1s]2p $^3P^o_1$	6.60E+08		3.44E+08	
2	3	[1s]2p $^1P^o_1$	3.93E+12		3.80E+12	
3	2	[1s]2s2p $^2P^o_{1/2}$	3.39E+12	6.60E+12	3.00E+12	7.53E+12
3	3	[1s]2s2p $^2P^o_{3/2}$	3.42E+12	5.76E+12	3.02E+12	6.96E+12
3	4	[1s]2s2p $^2P^o_{1/2}$	3.19E+11	7.56E+13	3.12E+11	6.67E+13
3	5	[1s]2s2p $^2P^o_{3/2}$	2.90E+11	7.60E+13	2.87E+11	6.73E+13
4	2	[1s]2p $^1P^o_1$	3.40E+12	9.10E+13	3.10E+12	8.15E+13
5	3	[1s]2p^2 $^2D_{5/2}$	1.34E+12	2.19E+14	1.22E+12	1.93E+14
5	4	[1s]2p^2 $^2D_{3/2}$	1.35E+12	2.18E+14	1.28E+12	1.92E+14
5	5	[1s]2p^2 $^2P_{1/2}$	4.31E+12	9.29E+13	4.05E+12	7.57E+13
5	6	[1s]2p^2 $^2P_{3/2}$	4.31E+12	9.30E+13	4.05E+12	7.58E+13
5	7	[1s]2p^2 $^2S_{1/2}$	1.63E+12	1.89E+14	1.50E+12	1.66E+14
6	6	[1s]2p^3 $^3D^o_3$	1.05E+12	2.37E+14	1.06E+12	2.11E+14
6	7	[1s]2p^3 $^3D^o_2$	1.05E+12	2.37E+14	1.06E+12	2.10E+14
6	8	[1s]2p^3 $^3D^o_1$	1.05E+12	2.37E+14	1.06E+12	2.10E+14
6	9	[1s]2p^3 $^3S^o_1$	4.81E+12	8.87E+13	4.81E+12	7.24E+13
6	10	[1s]2p^3 $^3P^o_2$	1.20E+12	2.22E+14	1.18E+12	1.98E+14
6	11	[1s]2p^3 $^3P^o_1$	1.20E+12	2.22E+14	1.18E+12	1.98E+14
6	12	[1s]2p^3 $^3P^o_0$	1.20E+12	2.22E+14	1.18E+12	1.98E+14
6	13	[1s]2p^3 $^1D^o_2$	3.46E+12	2.05E+14	3.46E+12	1.84E+14
6	14	[1s]2p^3 $^1P^o_1$	3.62E+12	1.90E+14	3.60E+12	1.71E+14
7	6	[1s]2p^4 $^4P_{5/2}$	8.67E+11	2.25E+14	9.35E+11	2.04E+14
7	7	[1s]2p^4 $^4P_{3/2}$	8.67E+11	2.25E+14	9.35E+11	2.04E+14
7	8	[1s]2p^4 $^4P_{1/2}$	8.68E+11	2.25E+14	9.35E+11	2.04E+14
7	9	[1s]2p^4 $^2D_{5/2}$	1.78E+12	2.60E+14	1.93E+12	2.44E+14
7	10	[1s]2p^4 $^2D_{3/2}$	2.46E+12	2.36E+14	1.96E+12	2.43E+14
7	11	[1s]2p^4 $^2P_{3/2}$	3.17E+12	2.10E+14	4.17E+12	1.73E+14
7	12	[1s]2p^4 $^2P_{1/2}$	3.85E+12	1.86E+14	4.20E+12	1.72E+14
7	13	[1s]2p^4 $^2S_{1/2}$	1.96E+12	2.43E+14	2.10E+12	2.28E+14
8	6	[1s]2p^5 $^3P^o_2$	1.39E+12	2.41E+14	1.70E+12	2.48E+14
8	7	[1s]2p^5 $^3P^o_1$	1.39E+12	2.41E+14	1.70E+12	2.48E+14
8	8	[1s]2p^5 $^3P^o_0$	1.39E+12	2.41E+14	1.70E+12	2.48E+14
8	9	[1s]2p^5 $^1P^o_1$	2.99E+12	2.20E+14	3.66E+12	2.29E+14

Table 9. Comparison of $\Delta E(2,3)^*$ for O ions

N	z	Present[a]	Expt	Other theory
8	1	1.06	1.06[b], 0.99[c]	1.02[e], 1.00[f]
7	2	1.93		
6	3	2.90		
5	4	3.73		
4	5	5.03		
3	6	5.64		
2	7	7.00	7.02[d]	
1	8	8.90	8.90[d]	

*Energy interval in Ryd between the lowest $n = 2$ and $n = 3$ resonances

[a]Approximation RM1 for $N > 2$ and AS1 for $N \leq 2$

[b]Photoionization experiment (Stolte et al. 1997)

[c]Photoabsorption measurements (Menzel et al. 1996)

[d]Spectroscopic tables (Moore 1998)

[e]R-matrix calculation (McLaughlin & Kirby 1998) with experimental thresholds of Krause (1994)

[f]R-matrix calculation (McLaughlin & Kirby 1998) with experimental thresholds of Stolte et al. (1997)